RSC Advances

ROYAL SOCIETY OF CHEMISTRY

www.rsc.org/advances

Direct coupling of unactivated alkynes and C(sp^3)−H bonds catalyzed by Pt(II, IV)-centered catalyst: A computational study

Zhi-Feng Li,[*,†,‡] Hui-Xue Li,[†] Xiao-Ping Yang,[†] Xin-Wen Liu,[†] Guo-Fang Zuo,[*,†] Cunyuan Zhao[*,‡]

[†]College of Life Science and Chemistry, Key Laboratory for New Molecule Design and Function of Gansu Universities, Tianshui Normal University, Tianshui 741001, China
[‡]School of Chemistry and Chemical Engineering, Sun Yat-Sen University, Guangzhou 510275, P. R. China

Email: *zflitsnu@163.com, zogofn@126.com, ceszhcy@mail.sysu.edu.cn*

Abstract: Direct coupling of unactivated alkynes and C(sp^3)−H bonds catalyzed by Pt(II, IV)-centered catalyst **X** (**X** = $PtCl_2$, $PtBr_2$, PtI_2 and PtI_4) (*J. Am. Chem. Soc.* **2009**, *131*, 16525) have been theoretically investigated with density functional theory (DFT). A comprehensive mechanistic DFT study of these reactions was carried out to better understand the experimental outcomes, and divergent and substrate-/catalyst-dependent mechanisms for the formation of ether derivatives were uncovered based on the computational results. Free energy diagrams for three types of mechanisms were computed, a) in **Mechanism I**, the transition state implies a directed 1,5-hydrogen shift (pathways ***a1-a4***), b) **Mechanism II** leads to formation of a Pt(II, IV) vinyl carbenoid (pathway ***b***), and c) **Mechanism III** with a O-coordinated Pt and including 5,6-hydrogen migration (pathway ***c***). Results suggest that the catalyzed mechanism with PtI_4 is different with the catalysts of $PtCl_2$, $PtBr_2$ and PtI_2. When $PtCl_2$, $PtBr_2$ and PtI_2 used the insertion reaction pathway ***a2*** is favored while PtI_4 adopted the pathway ***a1*** is reasonable. Comparing the energy profiles, the pathway ***a1*** with PtI_4 is the most favored. Through 1,5-hydrogen transfer, the

concerted insertion pathway ***a1*** with carbocationic intermediate is favored while the vinyl carbenoid mechanism is implausible.

1. INTRODUCTION

Carbon−carbon bond formation, a way to extend the carbonbackbone, is the fundamental reaction in organic synthesis. Although C-H bond functionalization with transition-metal catalyzed provides strategically new opportunities in carbon−carbon bond formation,[1-7] activation of C(sp^3)-H bonds is still considered a difficult challenge because of their high dissociation energy.[8, 9] To date, despite much effort has been devoted to C−C bond formation in the past decades, and significant progress in transition-metal catalysts which have emerged as an alternative to conventional C-C bond forming reactions through cleavage of activated or inactive C(sp^3)-H bonds, catalytic transformations of C(sp^3)-H bonds to C-C bonds with platinum (II, IV) catalysts still remain rare.[10-17]

Since the platinum(II)-catalyzed oxidation of methane to methanol[18], catalysis with Pt-salts is a rapidly evolving area of research for development of new reactions triggered by π-activation of alkynes and nowadays which has been initiated extensive investigation of C(sp^3)-H bond activation.[10-13, 19-23] Recently, Pt-centered catalysts have shown their efficiency in a series of transformations involving the transfer of a nucleophilic group onto an alkyne, followed by ring closure on the resulting carbocationic intermediate.[24-29] For example, Pt-catalyzed intramolecular hydroalkylation of unsaturated aryl alkynes provides convenient access to highly functionalized indenes.[10-13] Sames and co-workers reported a distinct reaction, in

which the unactivated terminal alkynes serve as hydride acceptors in *the through-space hydride transfer* and undergo catalytic intramolecular hydroalkylation at the α-position of saturated heterocyclic ethers, providing rapid access to bicyclic products.[30] The hydroalkylation of terminal alkynes has previously been limited to aromatic substrates and to give substituted indenes via an overall cyclization (**Scheme 1**).[10-12,31] Three types of mechanistic pathways of these formal cycloisomerizations were proposed: (1) the cycloisomerizations were proposed to proceed via the initial

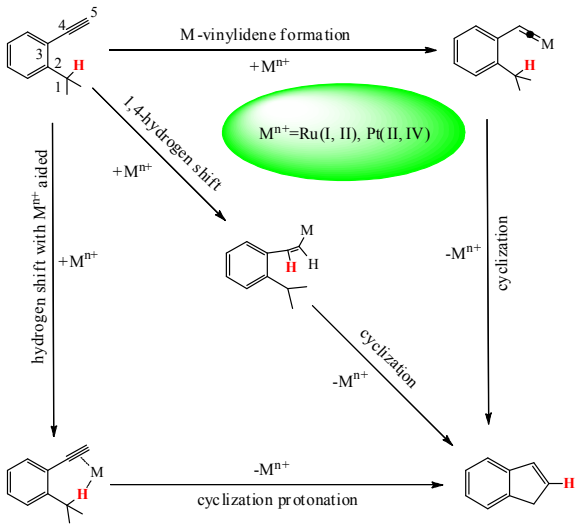

Scheme 1 Three plausible mechanisms were envisioned for novel M-catalyzed transformation

formation of a M-vinylidene species,[10-12] (2) a 1,4-hydrogen shift along the π-system[13, 14] and (3) a hydrogen shift with M^{n+} aided process.[13, 14, 32] The above three mechanisms were hypothesized based on the unsaturated aryl alkynes aromatic substrates. However, the calculated details for the rare examples of the intramolecular hydroalkylation at the α-position of saturated heterocyclic ethers, providing rapid access to bicyclic products are unclear. [30]

The remarkable progress in the hydroalkylation of terminal alkynes has mostly been focused on synthesis and characterization of new complexes, without utilizing computational chemistry to validate mechanistic speculation.[10-13, 33] Although a few groups have discussed the mechanism of this type of reaction[10-13, 23, 30] and previously, Zhao and co-workers[34] discussed several possible pathways of the bicyclic products formation from substrate **1** (**Scheme 2**) with PtI_4 as the catalyst, there are few detailed theoretical studies available in the literature where mechanistic possibilities are compared between the Pt(II)- and Pt(IV)-catalyzed transformation and why the different substrates **2** and **3** (**Scheme 2**) possessing the different yield (62% and 33% respectively) in experiment comparing to the substrate **1** (86%) is unclear.[10-13] Hence, in this paper, we present a thorough density functional theory (DFT) computational investigation of the mechanism of Pt(II,IV)-catalyzed synthesis of bicyclic

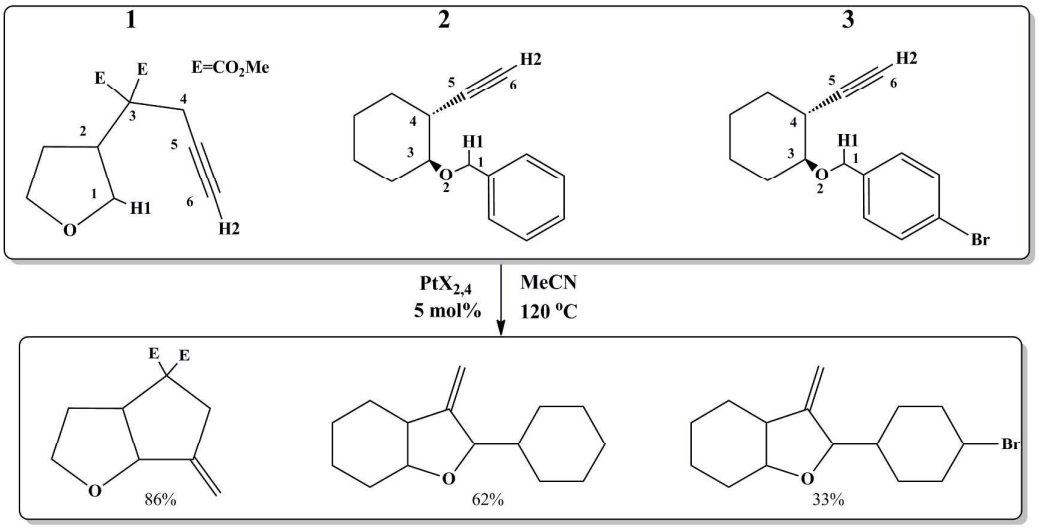

Scheme 2. The reaction schemes of substrates **1**, **2** and **3**

products through the intramolecular hydroalkylation at the α-position of saturated heterocyclic ethers substrates **1**, **2** and **3**.[30, 34]

We attempt to gain detailed insight on the catalytic mechanism by employing DFT calculations to examine the following aspects of the reaction: how the substrate and the catalyst bind to a complex, how the different substrates (substrates **1**, **2** and **3**) and the catalysts **X** (**X** = $PtCl_2$, $PtBr_2$, PtI_2 and PtI_4) effect on the mechanism of the reaction, the identity of the rate-limiting step of the whole transformation, whether or other reaction modes exist, such as O-coordinated Pt catalysis,[13, 32] and finally, whether or not the insertion mechanism is a stepwise or concerted process. Three plausible mechanisms (mechanism **I**, **II** and **III** in **Scheme 3**) were proposed. This will be referred to as the model substrate.[35]

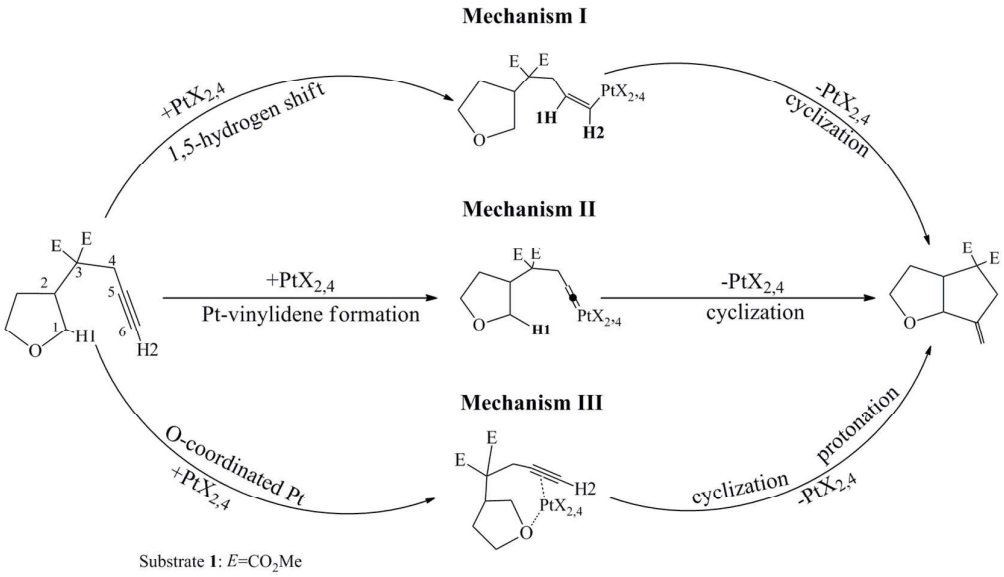

Scheme 3 Three plausible mechanisms were envisioned for this novel Pt-catalyzed transformation

2. COMPUTATIONAL METHODS

The geometries of all structures were fully optimized by density functional theory (DFT)[36] using the GAUSSIAN09 program suite.[37] We present here a combination of B3LYP[38-40](**L1**), ωB97X-D[41](**L2**) and M06-2X[42](**L3**) methods with

two basis sets [**BS1**: SDD for Pt and I, 6-31G(d) for the other atoms; **BS2**: SDD for Pt and I, 6-31G(d,p) for the other atoms] employed to obtain reliable geometries of complexes and the energy profiles because these computational methods have been successfully applied in the mechanistic studies of transition metal-catalysis.[14, 23, 43-48] Unscaled harmonic vibrational frequency calculations were used to characterize all of the stationary points as either minima or transition states. Intrinsic reaction coordinates (IRC)[49, 50] were employed to verify the connection of the transition states to two relevant minima. In some cases, in order to further verify the reliability of the key geometries and the processes on the pathway, we also calculated corresponding geometries at the higher calculated level, such as calculated level **L1/BS3** (**BS3**: SDD for Au and I, 6-31+G(d,p) for the other atoms).

The polarized continuum model (PCM)[51-53] with UFF sets of radii was applied and single-point energy calculations were done at the different calculated methods with basis set **BS4** (SDD for Au and I, 6-311++G(d,p) for the other atoms) using the geometries along the minimum energy pathway. The dielectric constant was assumed to be 36.6 for the bulk solvent MeCN. It can be seen from **Table S1** and **Table S2** (See ESI), although the tendency of calculated energy values at different calculated levels are qualitatively similar, the B3LYP method can severely underestimate the reaction barrier height.[48] Therefore, throughout the paper, we discuss only the results from the *ω*B97X-D /**BS1** [SDD for Pt and I, 6-31G(d) for the other atoms] level of theory.

3. RESULTS AND DISCUSSION

From the literature,[10-14, 25, 30, 32] we examined the detailed reaction mechanisms for Pt-catalyzed C(sp^3)-H activation/C-C bond formation reactions depicted in **Scheme 3**. A saturated heterocyclic ethers substrate of alkynes (substrate **1** in **Scheme 2**) was chosen as the first model system with $PtCl_2$, $PtBr_2$ and PtI_2 (denoted as **A**, **B** and **C** respectively) as catalysts as well as the substrates **1**, **2** and **3** with PtI_4 (denoted as **D**) as catalysts are secondly used in theory to study why the reaction active of the substrate **2** and **3** are weaker than that of substrate **1**. The substrates **1**, **2** and **3** are representative of experiments.[30] In the paper, the ***i*X-*x*-IN*n***/***i*X-*x*-TS*n*** denotes the ***n***th intermediate **IN*n***/transition state **TS*n*** on the pathway ***i*X-*x*** based on the substrate ***i*** and the catalyst **X** (***i*** = **1**, **2** and **3**; **X**= **A**, **B**, **C** and **D**; ***x*** = ***a***, ***b*** and ***c***).

3.1 Mechanism of cyclization of substrate 1 with different catalysts

Catalyzed by Catalyst A: $PtCl_2$. It is a generally accepted that the Pt-catalyzed cyclization begins from the coordination of Pt to the nucleophilic center/centers of the substrate. However, experimental evidence supporting the structure of the reactive intermediates is still lacking.[11-13, 30, 32] We therefore looked for the possible structures of such complexes. **Figure 1** and **Figure 2** show the optimized structures of two intermediates **1A-*a1*-IN1** (in pathway **1A-*a1***) and **1A-*a2*-IN1** (in pathway **1A-*a2***) corresponding to the initial coordination stage. It is observed that the Pt(II) in **1A-*a1*-IN1** and **1A-*a2*-IN1** are both attacked by the nucleophilic center alkyne group, as well as the H1 atom in **1A-*a1*-IN1** is over the alkyne group attribute to the 19.0° of

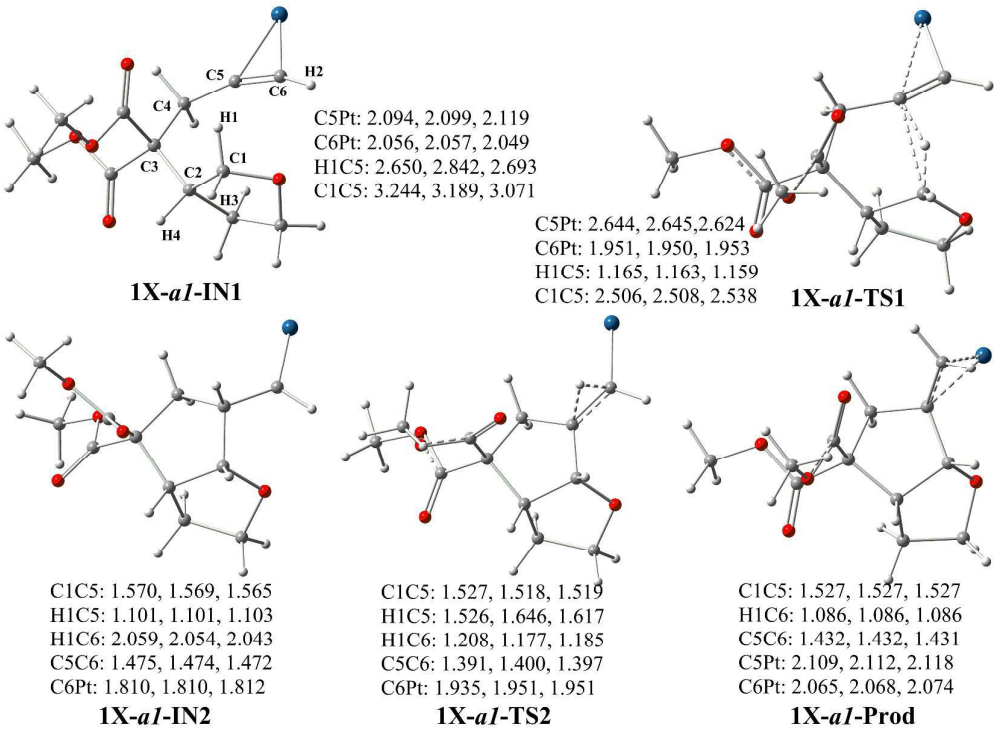

Figure 1. Schematic diagrams of the optimized geometries for the pathway **1X-*a1*** (parameters from left to right corresponding to **X** = **A**, **B** and **C** respectively, bond length: Å, angle: °)

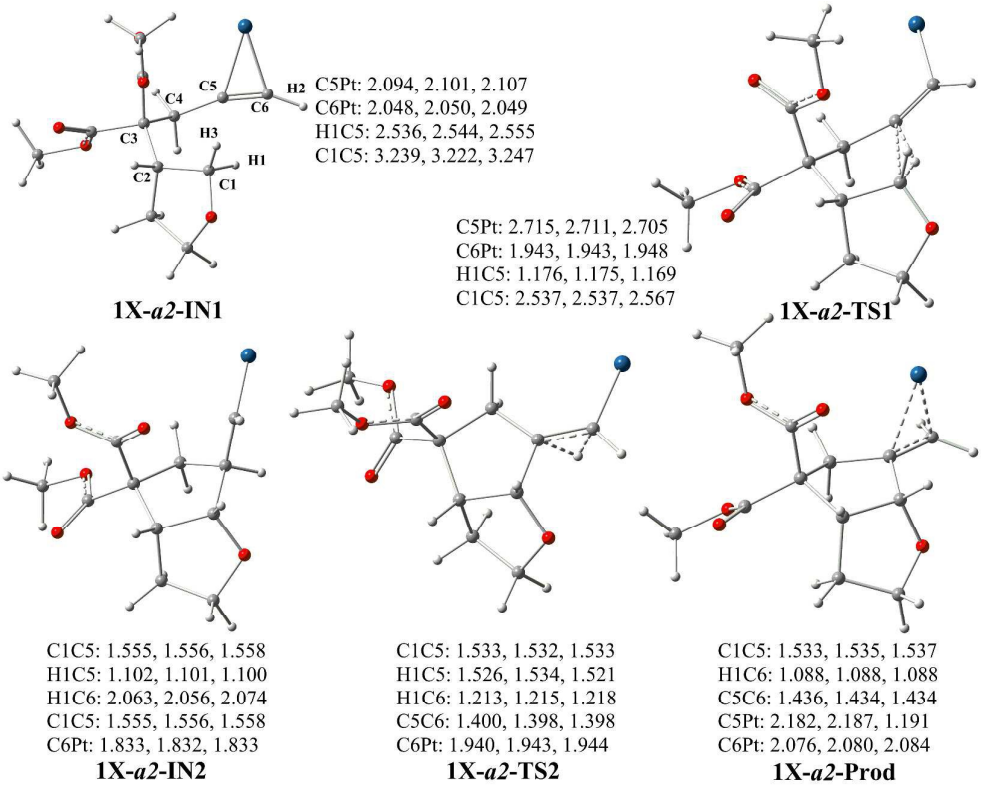

Figure 2. Schematic diagrams of the optimized geometries for the pathways **1X-*a2*** (parameters from left to right corresponding to **X** = **A**, **B** and **C** respectively, bond length: Å, angle: °)

the angle ∠H1C3C5C6, while in **1A-*a2*-IN1** the H1 atom is under the alkyne group (∠H1C3C5C6=-21.5°). These cases result in the 1,5-hydrogen shift easy occurred over the plane C3C5C6 in **1A-*a1*-IN1** whereas the 1,5-hydrogen migration under the plane C3C5C6 in **1A-*a2*-IN1**. In **1A-*a1*-TS1**, the distances between H1, C1 and C5 are decreased to 1.165 Å and 2.506 Å, while that between H1 and C1 is elongated by 0.070 Å (from 1.095 to 1.165 Å).

Figure 3 shows that the free energy of activation was calculated to be 18.0 kcal/mol for **1A-*a1*-TS1** and the free energy of reaction was -27.4 kcal/mol for the **1A-*a1*-IN2** with respect to **1A-*a1*-IN1**. The five-membered ring is formed in the **1A-*a1*-IN2**. Subsequently, the system is endothermic with 11.9 kcal/mol and crossed the transition state **1A-*a1*-TS2**, the product complex **1A-*a1*-P** is produced with exothermic 40.3 kcal/mol comparing to the intermediate **1A-*a1*-IN1**. In pathway **1A-*a1***, the energies of intermediate **1A-*a1*-IN2** and transition state **1A-*a1*-TS2** are at least lower by ~15 kcal/mol than that of the previous complex **1A-*a1*-IN1**. Therefore, although the energy barrier of the second 5,6-H shifting is reached to 11.9 kcal/mol, the rate-limiting step in pathway **1A-*a1*** is the first 1,5-H shifting process **1A-*a1*-IN1** → **1A-*a1*-TS1** → **1A-*a1*-IN2** with the energy barrier 18.0 kcal/mol.

As above mentioned, the catalyst $PtCl_2$ can also from under of plane C3C5C6 to attack the nucleophilic center of alkyne group and the **1A-*a2*-IN1** is formed. It is from **Figure 3**, in pathway **1A-*a2***, the energy of **1A-*a2*-IN1** is lower by 0.9 kcal/mol than that of the **1A-*a1*-IN1**. In **1A-*a2*-IN1**, the dihedral angle ∠H1C3C5C6 is -21.5° but it is 19.0° in **1A-*a1*-IN1**. Therefore, the H1 atom is posited under the alkyne group and

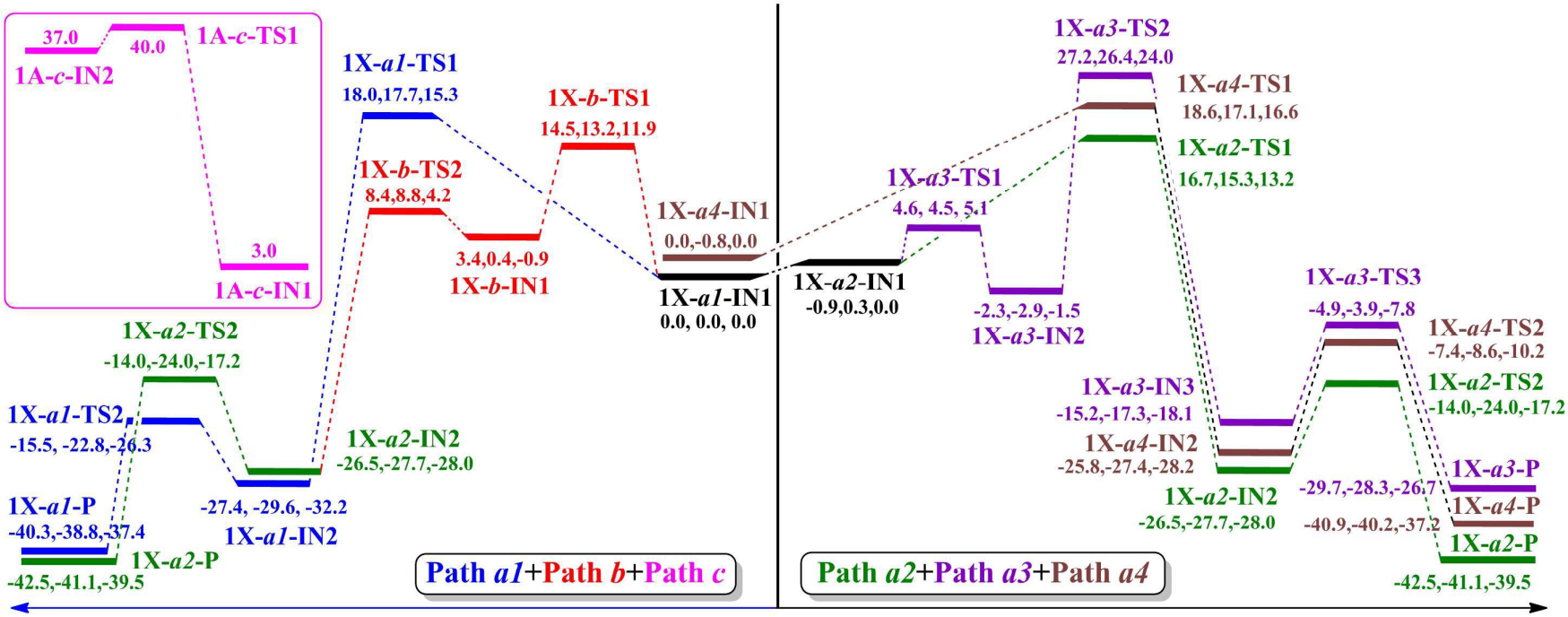

Figure 3. Energy profiles (kcal/mol) for pathways **1X-*a1, -a2, -a3, -a4***, **-*b*** and **-*c***. (The parameters from left to right corresponding to **X** = **A**, **B** and **C** respectively)

it is easy to shift from C1 to C5 through the under of the plane C3C5C6, and the transition state **1A-*a2*-TS1** distinctly exemplifies this character. In **1A-*a2*-TS1**, the distance between H1 and C5 is longer by 0.011 Å than that in **1A-*a1*-TS1** and the energy barriers of **1A-*a2*-TS1** is lower by 0.4 kcal/mol than that of **1A-*a1*-TS1**. The free energy of reaction was -25.6 kcal/mol for the **1A-*a2*-IN2** with respect to **1A-*a2*-IN1**. Initial from the intermediate **1A-*a2*-IN2**, the reaction process is similar to the pathway **1A-*a1***, they both involve the 5,6-H transferring transition states (**1A-*a2*-TS2** and **1A-*a1*-TS2** respectively). And also, although the energy barrier of **1A-*a2*-TS2** is reached to 12.5 kcal/mol, which is lower 5.0 kcal/mol than 17.5 kcal/mol of **1A-*a2*-TS1** and 11.7 kcal/mol than that of **1A-*a2*-IN1**. Therefore, the overall rate-limited step is not 5,6-H shifting, but 1,5-H transferring in pathway **1A-*a2***.

Overall, the intermediates, the transition states and the potential energy surfaces of pathway **1A-*a1*** and pathway **1A-*a2*** are similar. Both of them involve two intermediates and two transition states. The two hydrogen shifting processes are occurred from the upside of plane C3C5C6 in pathway **1A-*a1*** while in pathway **1A-*a2***, the underside of the plane C3C5C6 is favored for hydrogen migrating. Therefore, in 1,5-H shifting paths (pathways **1A-*a1*** and **-*a2***), the pathway **1A-*a2*** is more favored than pathway **1A-*a1***.

In Sames'[30] experimental and Zhao's[34] theoretical investigations, they both proposed that the H1 atom of substrate **1** can transfer from C1 atom to C5 and the product in which the H3 and H4 are in the same side of five-membered ring of ether.

However, they are not mentioned another impossible pathway **1A-*a3*** in which the H3 of substrate **1** may be migrate from C1 to C5 and in product the H3 and H4 are in the different side of five-membered ring of ether. In order to explore whether or not this process is exist, we first made the H3-C5 bond scan energy profile. It can be clearly found when H3 in **1A-*a2*-IN1** transferred from C1 to C5, there were two located maxima and three located minimum points in the scan energy profile (see **Figure S1** in ESI). Based on the scan energy profile, three intermediates (**1A-*a3*-IN1**, **1A-*a3*-IN2** and **1A-*a3*-IN3**) and two transition states (**1A-*a3*-TS1** and **1A-*a3*-TS2**) were obtained. The intermediates and the transition states in pathway **1A-*a3*** are listed in **Figure 4** and the energy profile is listed in **Figure 3**.

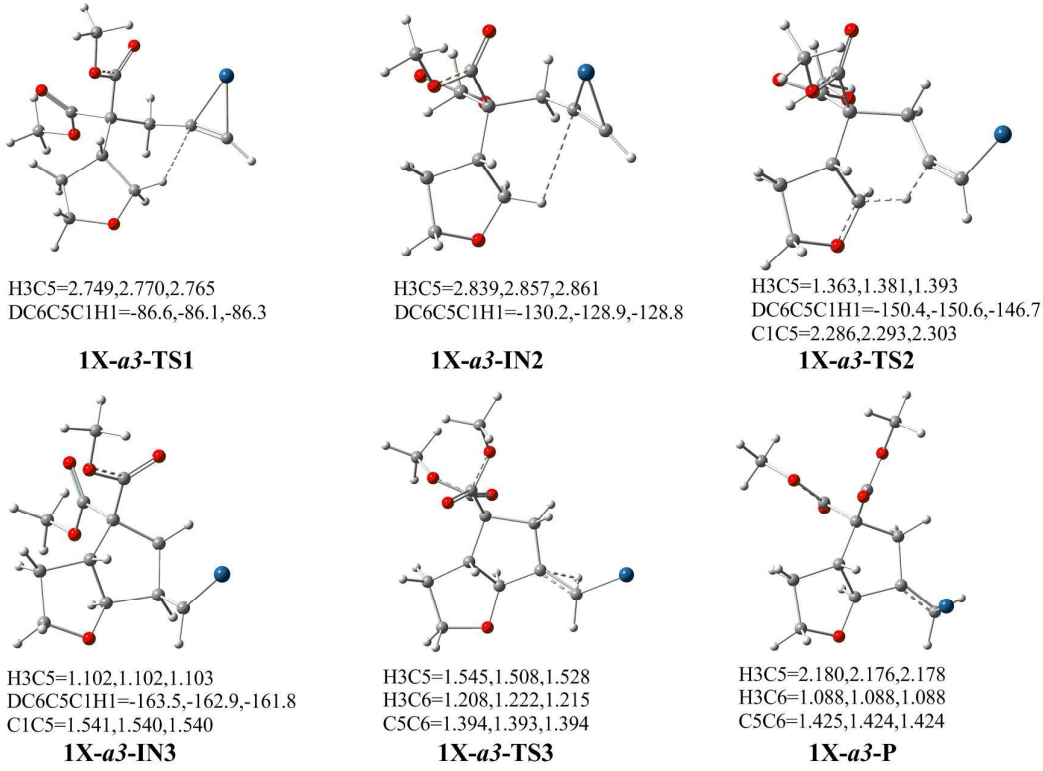

Figure 4. Schematic diagrams of the optimized geometries for the pathways **1X-*a3*** (parameters from left to right corresponding to **X** = **A**, **B** and **C** respectively, bond length: Å, angle: °)

From **Figure 3**, one can find that the pathways **1A-*a3*** and **1A-*a2*** has the same primarily **1A-*a2*-IN1**. The dihedral angle ∠C6C5C1H1 changes further along the mechanistic pathway, from -30.8° in **1A-*a2*-IN1** to -86.6° in **1A-*a3*-TS1**, and finally to -130.2° in **1A-*a3*-IN2**, when the dihedral rotation is completed. For the subsequent processes, although the **1A-*a3*-TS2** → **1A-*a3*-IN3** → **1A-*a3*-TS3** → **1A-*a3*-P** in pathway **1A-*a3*** are similar to **1A-*a2*-TS1** → **1A-*a2*-IN2** → **1A-*a2*-TS2** → **1A-*a2*-P** in pathway **1A-*a2*** (in both of them two H-transferring steps are involved), the relative energy/active energy of **1A-*a3*-TS2** in pathway **1A-*a3*** is higher by 10.5/11.9 kcal/mol than that of the **1A-*a2*-TS1** in pathway **1A-*a2***. Additionally, the product complex **1A-*a3*-P** is higher by 12.8 kcal/mol than the complex **1A-*a2*-P**. Therefore, the pathway **1A-*a3*** is unfavored whatever in thermodynamics or dynamics comparing to the pathway **1A-*a2*** and it may be ruled out.

Another mechanistic possibility considers because platinum-catalyzed cyclization of alkynes commonly occurs with accompanying migration of hydrogen or other groups.[13, 24-29] Yammamoto *et al*.[32] point out that the catalytic cyclization of *o*-alkynylbenzaldehyde acetals to functionalized indenes can be occur via catalyst-aided methoxy transfer. Also, He and coauthors[13] show that the intramolecular cyclization of *o*-substituted aryl alkynes through C(sp^3)-H activation can be completed via a catalyst-aided hydrogen shift process and which is further verified by our calculated investigation.[14] Inspired by these ideas, we take much time and try to explore a potential mechanistic scenario (catalyst-aided hydrogen shift mechanism) and the indirect catalyst-aided hydrogen shift pathway **1A-*a4*** is obtained.

From **Figure 3** and **Figure 5,** the pathway **1A-*a4*** is initialed from precursor **1A-*a4*-IN1**, in which the distance between H1 and Pt is 2.546 Å and possesses the weak interaction because of LP(Pt)→σ*(C1-H1) interaction ($E_{ij}^{(2)}$ = 0.84 kcal/mol).

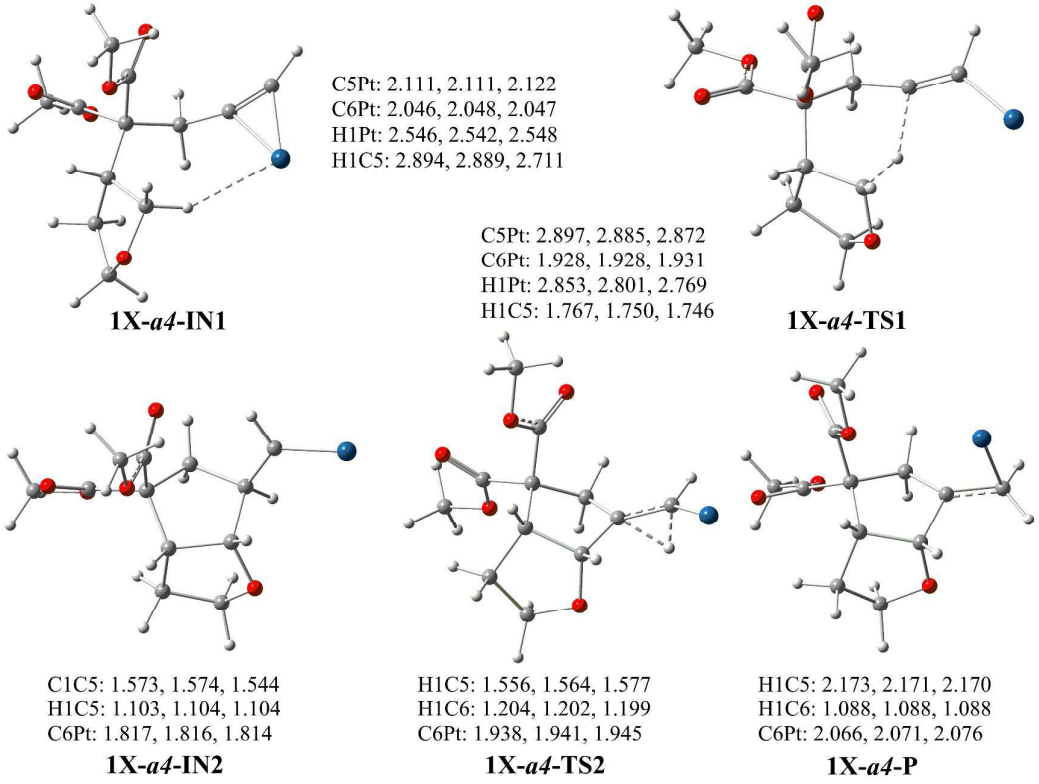

Figure 5. Schematic diagrams of the optimized geometries for the pathways **1X-*a4*** (parameters from left to right corresponding to **X** = **A**, **B** and **C** respectively, bond length: Å, angle: °)

With endothermic 18.6 kcal/mol, the transition state 1,5-H transition of **1A-*a4*-TS1** is concerted and the intermediate **1A-*a4*-IN2** is produced with exothermic 25.8 kcal/mol respect to **1A-*a4*-IN1**. Finally, with the 5,6-H transferring, the product complex **1A-*a4*-P** is produced. In pathway **1A-*a4***, the rate-limited step is 1,5-H shift process **1A-*a4*-IN1** → **1A-*a4*-TS1**→ **1A-*a4*-IN2** with the relative energy 18.6 kcal/mol compare to **1A-*a1*-IN1**, which is higher 1.9 kcal/mol than that of **1A-*a2*-TS1** with the same referenced **1A-*a1*-IN1**. This case indicates that the pathway **1A-*a4*** is not favored and the pathway **1A-*a2*** is occurred in the system.

It can be seen that the pathway **1A-*b*** has the same preliminary Pt-intermediate (**1A-*a1*-IN1**) with pathway **1A-*a1***. Pathway **1A-*b*** involves three hydrogen shifting process, 6,5-H, 1,6-H and 5,6-H shifting. The free energy barrier of directed 6,5-hydrogen shifting process (**1A-*b*-TS1**) is 14.5 kcal/mol. In **1A-*b*-TS1**, the distances between H2 and C5, C6 are 1.489 Å and 1.180 Å respectively, and the bond length of C5-C6 is decreased from 1.257 Å to 1.248 Å. With a exothermic process

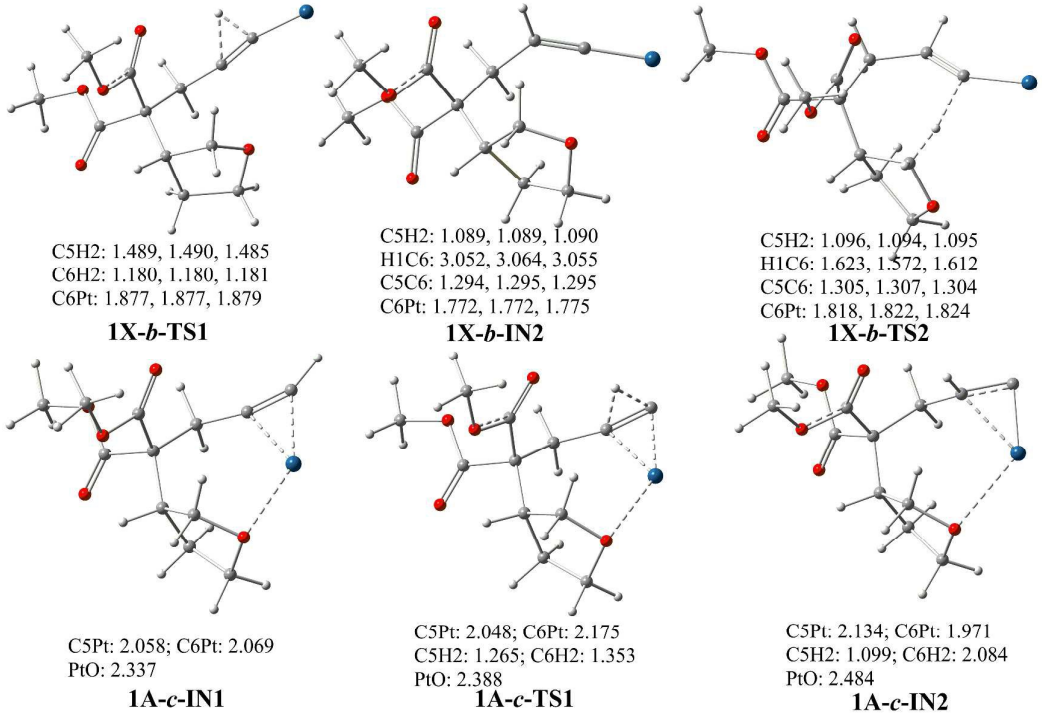

Figure 6. Schematic diagrams of the optimized geometries for the pathway **1X-*b*** and ***-c*** (parameters from left to right corresponding to **X** = **A**, **B** and **C** respectively, bond length: Å, angle: °)

1A-*b*-TS1 → **1A-*b*-IN1** (11.1 kcal/mol), the distance between C6 and Pt is decreased by 0.095 Å and the Pt-carbene intermediate **1A-*b*-IN1** is produced. The energy of **1A-*b*-IN1** is higher by 3.4 kcal/mol than that of the pre-complex **1A-*a1*-IN1**. The further process **1A-*b*-IN1** → **1A-*b*-TS2** → **1A-*a2*-IN2** is still involved the hydrogen

transferring (1,6-H shift) with energy barrier 5.0 kcal/mol and the free energy of **1A-*b*-TS2** is higher 8.4 kcal/mol than that of **1A-*a1*-IN1**. The reaction path of **1A-*b*** merges with pathway **1A-*a2*** at intermediate point **1A-*a2*-IN2**. Further, the **1A-*a2*-IN2** goes through **1A-*a2*-TS2** and the Pt-complex product **1A-*a2*-P** is generated, accompanied by the third hydrogen transferring (5,6-H shift). Overall, the energy barrier of the rate-limit step of pathway **1A-*b*** is 14.5 kcal/mol, although which is lower about 3 kcal/mol than that in **1A-*a2*** pathway, the free energy of the second transition state **1A-*b*-TS2** is higher 8.4 kcal/mol than their precursor **1A-*a1*-IN1** whereas the transition state **1A-*a2*-TS2** in pathway **1A-*a2*** is lower 14.0 kcal/mol than that of **1A-*a1*-IN1**. Therefore, the pathway **1A-*a2*** is favored.

On the other hand, excepting the nucleophilic center alkyne group, the transition metals can also attach the other nucleophilic atoms, such as O and N, which can promote the reaction going on.[32] Similar to this case, the pathway **1A-*c*** in which the Pt attached the O of substrate is existed in our studied system (**Figure 6** and **Figure 3**). First, the active centre Pt of $PtCl_2$ is attached both with the alkyne group and the O atom of heterocyclic five-membered ring and further the previous intermediate **1A-*c*-IN1** is produced. Comparing to intermediate **1A-*a1*-IN1** in pathway **1A-*a1***, the **1A-*c*-IN1** in pathway **1A-*c*** is 3.0 kcal/mol higher in energy than that of **1A-*a1*-IN1**. The energy barrier of 6,5-H shifting transition state **1A-*c*-TS1** is reached to 37.0 kcal/mol, which is about two times of the pathway **1A-*a2***. Therefore, the pathway **1A-*c*** is not favored and will be not discussed in detail below.

Overall, there are six reaction paths when $PtCl_2$ is used to catalyze the substrate **1**.

Pathways **1A-*a1*** to **1A-*a4*** are all involved two H-transferring processes. In pathway **1A-*b***, the Pt-carbene is produced and the three H-transferring processes is involved. As for the sixth pathway **1A-*c***, the Pt-centre is both attached by alkyne group and O atom of heterocyclic five-members ring and in which the rate-limited energy is highest than the other five pathways. Therefore, the **1A-*a2*** is the favored reaction pathway among six pathways. The step of C5 inserted the C1-H1 in pathway **1A-*a2*** is concerted, but stepwise mechanism in experimental is speculated.

Catalyzed by Catalysts B and C: $PtBr_2$ and PtI_2. Similar to $PtCl_2$ catalyzed pathways, there are six subpaths, including four pathways **1X-*a*** (***a1-a4***), one pathway **1X-*b*** and one pathway **1X-*c*** (**X = B and C**). The optimized geometries of intermediates, transition states and products and the selected parameters for these pathways are represented in **Figure 1**, **Figure 2** and **Figures 4-6**, the energy profiles for these processes are illustrated in **Figure 3**. In this section with the **B** and **C** as the catalysts, the active energies of favored subpaths are only discussed and compared because the geometries on them are very similar to those on pathways with $PtCl_2$ as catalyst. As for the same substrate **1**, the active energies of favored pathways **1X-*a2*** with different catalysts $PtCl_2$, $PtBr_2$ and PtI_2 are 17.6 kcal/mol, 15.0 kcal/mol and 13.2 kcal/mol respectively, this case indicates that the catalyzed capacity of catalyst **X** is decreased in the order PtI_2 > $PtBr_2$ > $PtCl_2$, which is agreement with Sames' experimental results. Although the energy barriers of pathway **1X-*b*** are lower about 1-3 kcal/mol than those of pathway **1X-*a2***, the energies of the second transition state **1X-*b*-TS2** in pathway **1X-*b*** are higher about 4-9 kcal/mol than the precursor

1X-*a1*-IN1. Therefore, as for **1X** (**X** = **A**, **B** and **C**) system, the **1X-*a2*** pathway is favored. Also, the inserted processes for C5 with C1-H1 in pathway **1X-*a2*** with $PtBr_2$ and PtI_2 are both concerted, which is similar to the pathway **1A-*a2*** with catalyst $PtCl_2$ and different from the experimental speculation.

Catalyzed by Catalyst D: PtI_4. The reaction of substrate **1** with the catalyst **X** = PtI_4 is investigated. The optimized geometries for the reactants, intermediates, transition states and product complex of the pathways are depicted schematically in **Figure 7**, the energy profile is illustrated in **Figure 8**.

As **Figure 7** and **Figure 8** showing, the pathway include two subpaths, one is pathway **1D-*a*** and another is pathway **1D-*b***. The pathway **1D-*a*** is similar to pathway **1X-*a1*** with $PtCl_2$, $PtBr_2$ and PtI_2 as catalysts, involving processes of the 1,5-H transferring of H1 atom, forming the five-membered ring between C1 and C5 atoms and the 5,6-H transferring of H1, and also the insertion of the C5 with C1-H1 is concerted. It is different from pathways with $PtCl_2$, $PtBr_2$ and PtI_2 as catalysts, the pathway **1D-*a*** with catalyst PtI_4 is similar to pathway **1X-*a1*** (**X** = **A**, **B** and **C**) is only obtained, which displays that the H1 atom transferred through the up of the plane C3C5C6 whereas the H1 atom transferred through under of C3C5C6 plane is not exist in theory, when used PtI_4 as catalyst.

Another pathway **1D-*b*** is similar to pathway **1X-*b*** (**X** = **A**, **B** and **C**) with $PtCl_2$, $PtBr_2$ and PtI_2 as catalysts, the product complex **1D-P** is produced with the sequence 6,5-H transferring (**1D-*b*-TS1**, Pt-carbenoid formed) → 1,6-H transferring (**1D-*b*-TS2**, five-membered ring formed) → 5,6-H transferring (**1D-*b*-TS3**, **1D-P** formed).

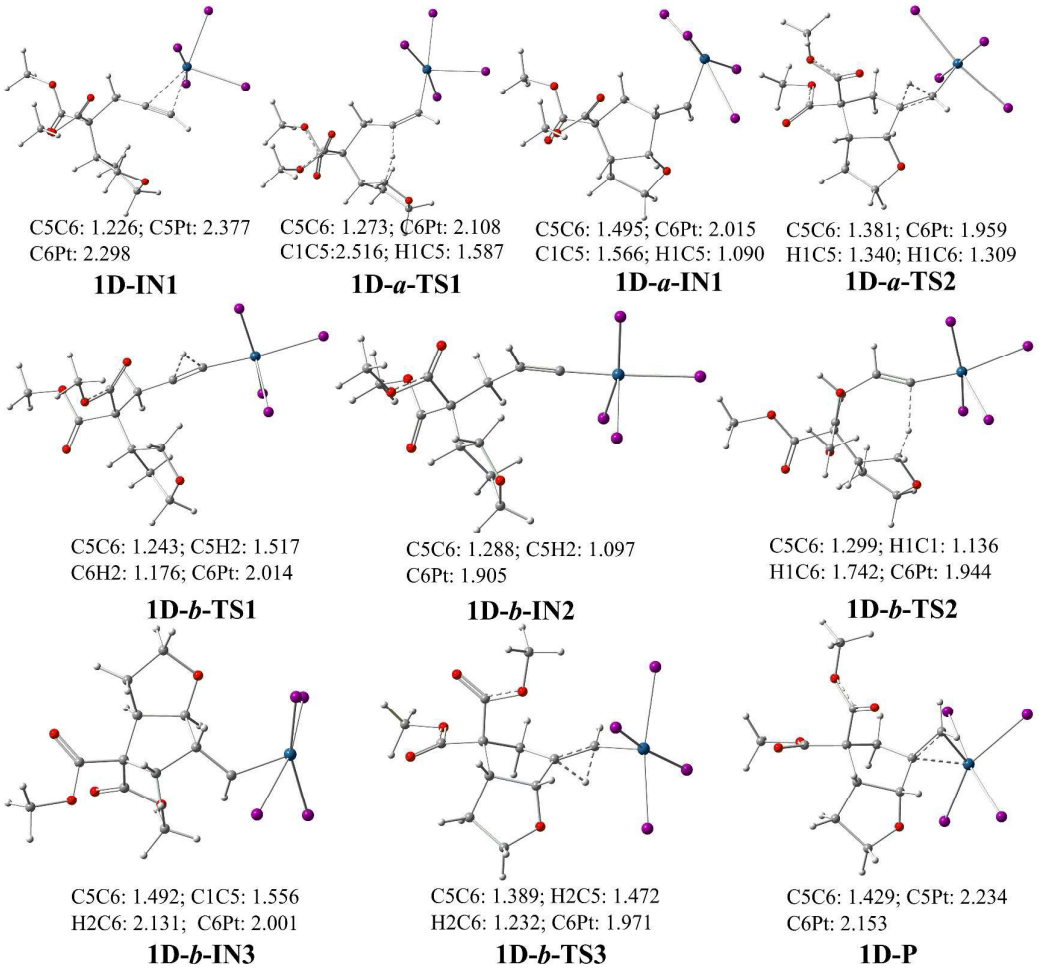

Figure 7. Schematic diagrams of the optimized geometries for the pathways **1D-*a*** and **-*b*** (bond length: Å, angle: °)

It can be seen from **Figure 8**, pathways **1D-*a*** and **-*b*** have the same initial complex **1D-IN1** and the active energy of limited-rate in pathway **1D-*a*** is lower (2.5 kcal/mol) than that of pathway **1D-*b***. And also, the energy of **1D-*b*-TS1** is higher 7.4 kcal/mol than that of **1D-*a*-TS1**. Therefore, the favored reaction path of substrate **1** with PtI_4 is pathway **1D-*a***.

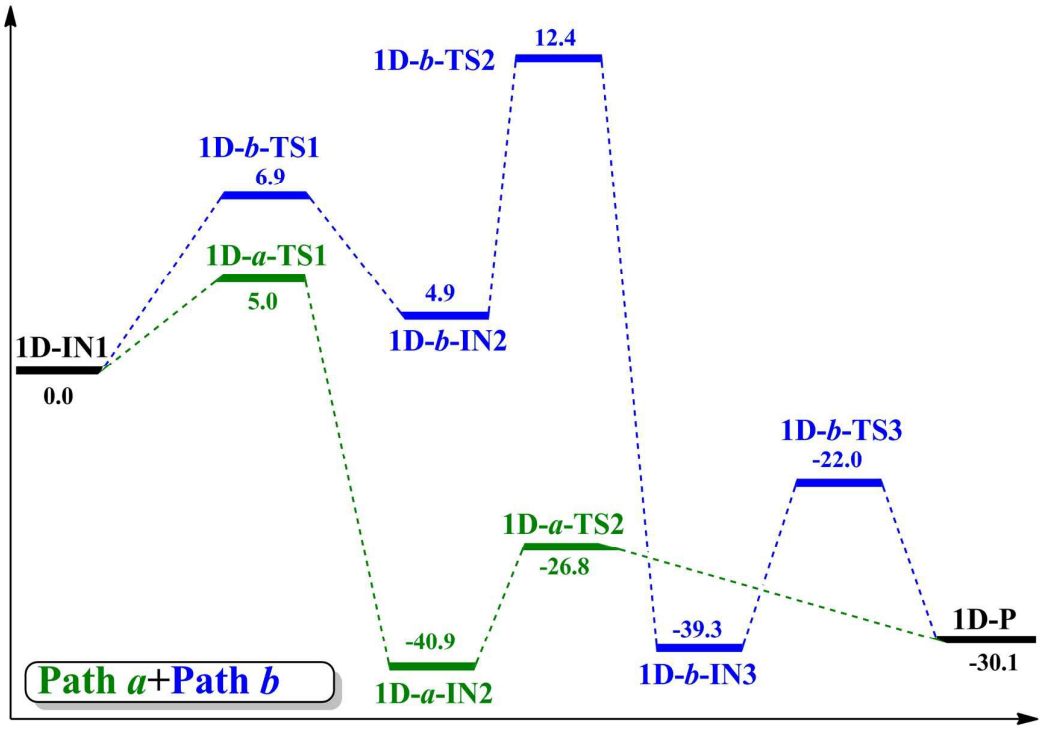

Figure 8. Energy profiles (kcal/mol) for pathways **1D-*a*** and **-*b***.

It can be concluded from above results and discussions, the substrate **1** can be coupled through varies reaction paths, including pathways **1X-*a***, **-*b*** and **-*c***. When $PtCl_2$, $PtBr_2$ and PtI_2 are used as catalyst, pathway **1X-*a2*** is favored, and when PtI_4 is used the pathway **1D-*a*** which is similar to pathway **1X-*a1*** (**X** = **A**, **B** and **C**) is more favored than the pathway **1D-*b***. Comparing to the pathways with $PtCl_2$, $PtBr_2$ and PtI_2 as catalyst, the active energy of **1D-*a*** based on PtI_4 is the lowest. Therefore, the PtI_4 is the most effective catalyst than the other catalysts $PtCl_2$, $PtBr_2$ and PtI_2 when the substrate **1** is used, which is consistent with the literature results. It is also seen from **Figures 1-9**, the 1,5-H and 1,6-H shift are all concerted in calculations,[54] which is different from the stepwise speculation in experiment.

3.2 Mechanism of the cyclization of substrates *i* = 2 and 3

The substrates **2** and **3** are used to investigate how the substrates effect on the reaction mechanism with effective catalyst PtI_4. The energy profiles are showed in

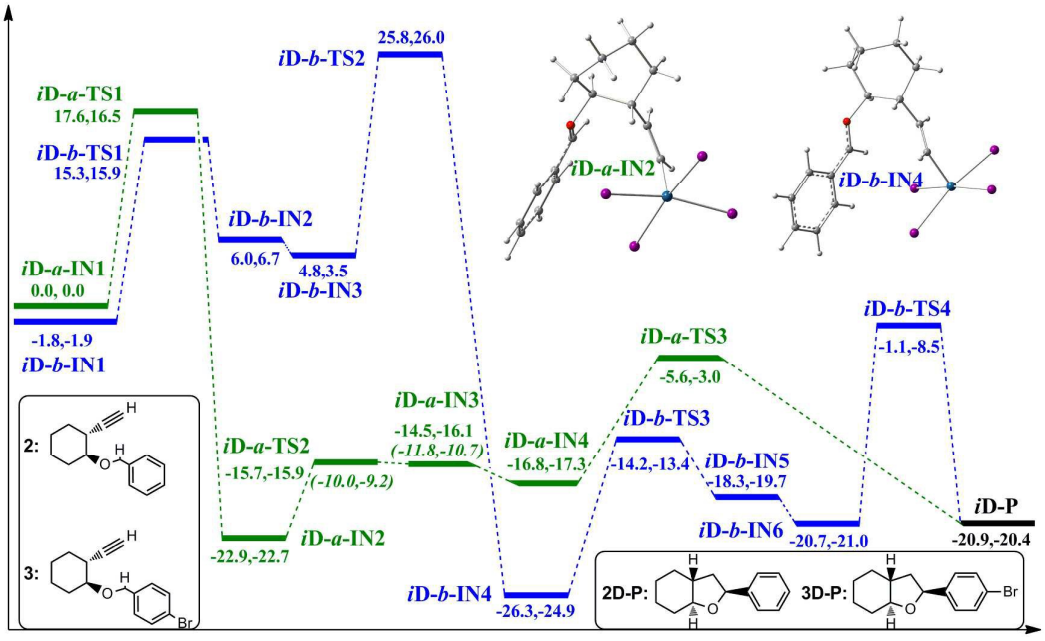

Figure 9. Energy profiles (kcal/mol) for pathways ***i*D-*a*** and ***-b*** (***i*** = **2**, **3**. Parameters from left to right corresponding to ***i*** = **2** and **3** respectively, the energies in italic are at M06-2X calculated method).

Figure 9. It can be seen that the pathways with substrates **2** and **3** are the same, one is 1,5-H shift pathway (**2**,**3**)**D-*a*** and the other is Pt-vinyl pathway (**2**,**3**)**D-*b***. The active energies of pathway (**2**,**3**)**D-*b*** are higher about 5 kcal/mol than those of pathway (**2**,**3**)**D-*a*** as well as the energies of rate-limited transition states **(2,3)D-*b*-TS2** are higher about 10 kcal/mol than those of **(2,3)D-*a*-TS1**. Therefore, the pathway (**2**,**3**)**D-*a*** is favored either for substrate **2** or **3** and the product in literature are obtained mainly through it. The pathway (**2**,**3**)**D-*a*** (involving two process of H-transferring) and pathway (**2**,**3**)**D-*b*** (involving intermediate of Pt-vinyl and three process of H-transferring) are similar to pathways **1D-*a*** and ***-b*** respectively. Different form the pathways **1D-*a*** and ***-b***, 1,5-H/1,6-H shifting of α-C(sp^3)-H in pathways **(2,3)D-*a*** and

-b is stepwise but concerted as well as the carbocation intermediate is existed[30] (see geometry schemes ***i*D-*a*-IN2** and ***i*D-*b*-IN4** in **Figure 9, *i* = 2**, **3**). By comparing the energy profiles illustrated in **Figures 3**, **8** and **9**, as for the same substrate **1**, the catalytic capability of PtI_4 among four catalysts ($PtCl_2$, $PtBr_2$, PtI_2 and PtI_4) is the most energetic. As for the different substrates **1**, **2** and **3**, the catalyzed capability of PtI_4 is decreased successively. The Br substituted on phenyl group is disfavored for the reaction, which is consistent with the results of the experiment.

4. CONCLUSION

Direct coupling of unactivated alkynes and C(sp^3)−H bonds catalyzed by platinum(II, IV)-centered catalyst is investigated. Three types of mechanism, one with a transition state structure of directed 1,5-hydrogen shift (**Mechanism I**), one that leads to the formation of Pt(II,IV) vinyl carbenoid (**Mechanism II**), and one with O-coordinated Pt involving 5,6-hydrogen migration (**Mechanism III**) were investigated by using Density Functional Theory. Our results indicate that:

The reaction activity of title system is much catalyst-dependent. The catalytic capacity of the $PtCl_2$, $PtBr_2$, PtI_2 and PtI_4 is increased successively and the reaction mechanism is rational. As for the substrate **1** with catalysts $PtCl_2$, $PtBr_2$ and PtI_2, the pathway **1X-*a2*** with the 1,5-H transferring through the under C3C5C6 plane is favored and the first insertion step of the C-H is concerted whereas the other pathways, including **1X-*a1*** (1,5-H transferring through the upside of the plane C3C5C6), pathway **1X-*a3*** (the transferred H in the another side of five–membered ring of ether), pathway **1X-*a4*** (indirect catalyst-aided hydrogen shift), pathway **1X-*b*** (5,6-H

transferring path) and pathway **1X-*c*** (O-coordinated Pt path) are secondary.

The reaction activity of title system is also much substrate-dependent. The catalyzed mechanism of PtI_4 with substrates **1**, **2** and **3** is different. As for substrate **1**, there are two types of reaction pathway, one is pathway **1D-*a*** which is similar to pathway **1(A**, **B**, **C)-*a1*** and another is pathway **1D-*b*** which is similar to pathway **1(A**, **B**, **C)-*b***. The pathways **2D-*a*/3D-*a*** and **2D-*b*/3D-*b*** with substrates **2**/**3** are different from the pathways **1D-*a*** and **1D-*b*** with substrate **1** respectively. The reaction barrier of pathway **1D-*a*** is lower than those of pathways **(2**,**3)D-*a*** and **-*b***, which results in the high yield of **1D-*a*-P** comparing to **(2**,**3)D-P**.

The 1,5-H/1,6-H shift is concerted which is verified by versatile computational levels, which is conflicted with the stepwise speculation in experiment. The theoretical investigation of this paper would strongly increase the predictive power and lead to improved rational relative catalyst design.

Acknowledgments

This work was supported by the National Natural Science Foundation of China (Grant No. 21463023, 21465021, 21373277), QingLan Talent Engineering Funds of Tianshui Normal University and the Foundation of Key Laboratory for New Molecule Design and Function of Gansu Universities. We thank the Gansu Computing Center, the high-performance grid computing platform of Sun Yat-Sen University and Guangdong Province Key Laboratory of Computational Science for generous computer time.

Notes and References

Electronic Supplementary Information (ESI) available: The complete citation for ref 37, the Cartesian coordinates for the calculated stationary structures at calculated levels are given. see DOI: xxx/xxx/.

1. Y. Guo, X. M. Zhao, D. Z. Zhang and S. I. Murahashi, *Angew. Chem., Int. Ed.*, 2009, **48**, 2047-2049.
2. Y. X. Jia and E. P. Kundig, *Angew. Chem., Int. Ed.*, 2009, **48**, 1636-1639.
3. N. Nebra, J. Lisena, N. Saffon, L. Maron, B. Martin-Vaca and D. Bourissou, *Dalton T*, 2011, **40**, 8912-8921.
4. S. Fantasia, A. Pasini and S. P. Nolan, *Dalton T*, 2009, 8107-8110.
5. V. Ritleng, C. Sirlin and M. Pfeffer, *Chem. Rev.*, 2002, **102**, 1731-1770.
6. S. Conejero, M. Paneque, M. L. Poveda, L. L. Santos and E. Carmona, *Acc. Chem. Res.*, 2010, **43**, 572-580.
7. F. Kakiuchi, S. Kan, K. Igi, N. Chatani and S. Murai, *J. Am. Chem. Soc.*, 2003, **125**, 1698-1699.
8. R. A. Periana, D. J. Taube, S. Gamble, H. Taube, T. Satoh and H. Fujii, *Science*, 1998, **280**, 560-564.
9. M. S. Chen and M. C. White, *Science*, 2007, **318**, 783.
10. G. B. Bajracharya, N. K. Pahadi, I. D. Gridnev and Y. Yamamoto, *J. Org. Chem.*, 2006, **71**, 6204-6210.
11. A. Odedra, S. Datta and R.-S. Liu, *J. Org. Chem.*, 2007, **72**, 3289-3292.
12. M. Tobisu, H. Nakai and N. Chatani, *J. Org. Chem.*, 2009, **74**, 5471-5475.
13. S. Yang, Z. Li, X. Jian and C. He, *Angew. Chem., Int. Ed.*, 2009, **48**, 3999-4001.
14. Z.-F. Li, Y. Fan, N. J. DeYonker, X. Zhang, C.-Y. Su, H. Xu, X. Xu and C. Zhao, *J. Org. Chem.*, 2012, **77**, 6076-6086.
15. J. M. Lee and S. Chang, *Tetrahedron Lett.*, 2006, **47**, 1375-1379.
16. L. C. Kao and A. Sen, *J. Chem. Soc., Chem. Commun.*, 1991, 1242-1243.
17. B. D. Dangel, J. A. Johnson and D. Sames, *J. Am. Chem. Soc.*, 2001, **123**, 8149-8150.
18. N. F. Goldshleger, V. V. Eskova, A. E. Shilov and A. A. Shteinman, *Zh. Fiz. Khim*, 1972, **46**, 1353.
19. A. R. Chianese, S. J. Lee and M. R. Gagne, *Angew. Chem., Int. Ed.*, 2007, **46**, 4042-4059.
20. M. P. Jensen, D. D. Wick, S. Reinartz, P. S. White, J. L. Templeton and K. I. Goldberg, *J. Am. Chem. Soc.*, 2003, **125**, 8614-8624.
21. S. M. Kloek and K. I. Goldberg, *J. Am. Chem. Soc.*, 2007, **129**, 3460-3461.
22. V. R. Ziatdinov, J. Oxgaard, O. A. Mironov, K. J. H. Young, W. A. Goddard Iii and R. A. Periana, *J. Am. Chem. Soc.*, 2006, **128**, 7404-7405.
23. Y. Wang, W. Liao, G. Huang, Y. Xia and Z.-X. Yu, *J. Org. Chem.*, 2014, **79**, 5684-5696.
24. Y. Zou, D. Garayalde, Q. Wang, C. Nevado and A. Goeke, *Angew. Chem., Int. Ed.*, 2008, **47**, 10110-10113.
25. I. Nakamura, G. B. Bajracharya, H. Wu, K. Oishi, Y. Mizushima, I. D. Gridnev and Y. Yamamoto, *J. Am. Chem. Soc.*, 2004, **126**, 15423-15430.
26. S. E. An, J. Jeong, B. Baskar, J. Lee, J. Seo and Y. H. Rhee, *Chem. Eur. J.*, 2009, **15**, 11837.
27. I. Nakamura, G. B. Bajracharya, Y. Mizushima and Y. Yamamoto, *Angew. Chem., Int. Ed.*,

2002, **41**, 4328-4331.
28. S. Wang and L. Zhang, *J. Am. Chem. Soc.*, 2006, **128**, 14274-14275.
29. P. Dubé and F. D. Toste, *J. Am. Chem. Soc.*, 2006, **128**, 12062-12063.
30. P. A. Vadola and D. Sames, *J. Am. Chem. Soc.*, 2009, **131**, 16525-16528.
31. J. Barluenga, M. Fañanás-Mastral, F. Aznar and C. Valdés, *Angew. Chem., Int. Ed.*, 2008, **47**, 6594-6597.
32. I. Nakamura, Y. Mizushima, I. D. Gridnev and Y. Yamamoto, *J. Am. Chem. Soc.*, 2005, **127**, 9844-9847.
33. X. Wu, S.-S. Chen, Y. Hu and L.-Z. Gong, *Org. Lett.*, 2014, **16**, 3820-3823.
34. L. Jin, Y. Wu and X. Zhao, *Organometallics*, 2012, **31**, 3065-3073.
35. As a model, it is suitable to study whether the -O- of saturated heterocyclic ethers and the carbon-carbon triple bond can both coordinate with Pt in initial intermediate.
36. R. G. Parr and W. Yang, *Density-functional Theory of Atoms and Molecules; Oxford Univ. Press: Oxford, 1989.*
37. M. J. Frisch, G. W. Trucks, G. W. Schlegel and G. W. Scuseria, *Gaussian 09, Revision D.01; Gaussian, Inc., Wallingford CT, 2013*.
38. A. D. Becke, *Phys. Rev. A*, 1988, **38**, 3098-3100.
39. C. Lee, W. Yang and R. G. Parr, *Phys. Rev. B*, 1988, **37**, 785.
40. A. D. Becke, *J. Chem. Phys.*, 1993, **98**, 5648.
41. J.-D. Chai and M. Head-Gordon, *Phys. Chem. Chem. Phys.*, 2008, **10**, 6615-6620.
42. Y. Zhao and D. Truhlar, *Theor. Chem. Acc.*, 2008, **120**, 215-241.
43. O. N. Faza, C. S. López, R. Álvarez and A. R. de Lera, *J. Am. Chem. Soc.*, 2006, **128**, 2434-2437.
44. F.-Q. Shi, X. Li, Y. Xia, L. Zhang and Z.-X. Yu, *J. Am. Chem. Soc.*, 2007, **129**, 15503-15512.
45. Z.-X. Yu, P. A. Wender and K. N. Houk, *J. Am. Chem. Soc.*, 2004, **126**, 9154-9155.
46. Z.-F. Li, X.-P. Yang, L. Hui-Xue and Z. Guo, *Organometallics*, 2014, **33**, 5101-5110.
47. T. Zhou and Y. Xia, *Organometallics*, 2014, **33**, 4230-4239.
48. A. J. Cohen, P. Mori-Sánchez and W. Yang, *Chem. Rev.*, 2012, **112**, 289-320.
49. K. Fukui, *Acc. Chem. Res.*, 1981, **14**, 363-368.
50. K. Fukui, *J. Phys. Chem.*, 1970, **74**, 4161-4163.
51. T. Mineva, N. Russo and E. Sicilia, *J. Comput. Chem.*, 1998, **19**, 290.
52. M. Cossi, G. Scalmani, N. Rega and V. Barone, *J. Chem. Phys.*, 2002, **117**, 43.
53. J. Tomasi and M. Persico, *Chem. Rev.*, 1994, **94**, 2027.
54. In order to verify these character, the corresponding 1,5-H/1,6-H shif transition states are optmized at higher theory level B3LYP/6-31+G(d,p)(SDD for I and Pt). Also, the IRC are performed at the same level and schemes are showed in ESI.The results further show they are concerted rather than stepwise in litherature speculateded.